ELSEVIER

Journal of Structural Geology 28 (2006) 641–653

JOURNAL OF STRUCTURAL GEOLOGY

www.elsevier.com/locate/jsg

Magma flow and thermal contraction fabric in tabular intrusions inferred from AMS analysis. A case study in a late-Variscan folded sill of the Albarracín Massif (southeastern Iberian Chain, Spain)

A. Gil-Imaz [a,*], A. Pocoví [a], M. Lago [a], C. Galé [a], E. Arranz [a], C. Rillo [b], E. Guerrero [b]

[a] *Departamento de Ciencias de la Tierra, Universidad de Zaragoza, C/Pedro Cerbuna 12, Zaragoza 50009, Spain*

[b] *Instituto de Ciencia de Materiales de Aragón (ICMA), Centro Superior de Investigaciones Científicas (CSIC)-Universidad de Zaragoza (UZ), Zaragoza, Spain*

Received 9 April 2005; received in revised form 9 December 2005; accepted 20 December 2005
Available online 14 March 2006

Abstract

The effects of different petrological processes on the rock fabric of a folded sill from the Albarracin Massif (southeastern Iberian Chain, Spain) were studied by means of the anisotropy of magnetic susceptibility (AMS) technique. The most outstanding feature of the sill at outcrop-scale is a network of joints linked to thermal contraction, which define polygonal columns. The analysis of the magnetic fabric, taking the orientation of sill walls and column axes as a reference and using the 'restored' directional data corresponding to the whole of *K*3 susceptibility axes, has revealed magnetic fabrics related to two processes: (a) magma flow with a SW-trending flow vector characterized by a curved geometry of the magma foliations and (b) thermal contraction coeval to lava cooling. Early magnetite crystals, grown in a relatively high viscosity calc-alkaline magma, are the main carriers involved in the AMS fabric. Passive rotation of the early magnetic mineralogy within a medium-viscosity magma explains the magnetic fabric linked to both magma flow and near-solidus thermal contraction of the magma. Late-Variscan folding of the sill produced the rigid-body reorientation of the magnetic fabric.

Keywords: Anisotropy of magnetic susceptibility; Magma flow; Thermal contraction; Late-Variscaan sill; Iberian Chain

1. Introduction

The anisotropy of magnetic susceptibility (AMS) technique has proved to be a valuable tool for defining magma flow directions in tabular intrusions such as dykes and sills (Ellwood, 1978; Hillhouse and Wells, 1991; Ernst and Baragar, 1992; Cañón-Tapia et al., 1996; Glen et al., 1997; Geoffroy et al., 2002) but few AMS studies have focussed on characterizing the effects of cooling on igneous rock fabrics (Brown et al., 1964; Ellwood and Fisk, 1977; Ellwood, 1979; Urrutia-Fucugauchi et al., 1991).

Two general models describe the relationship between magma flow direction and principal susceptibility axes. The classical application of the AMS technique to igneous rocks assumes that the magnetic lineation (or the mean of the *K*2 axes) is parallel to the magma flow vector (Knight and Walker, 1988; Rochette et al., 1991; Staudigel et al., 1992; Varga et al., 1998; Herrero-Bervera et al., 2001). In the second model, the flow vector is estimated from the geometric computation between the *K*3 axes and the pole of the intrusion wall (Hillhouse and Wells, 1991; Geoffroy et al., 2002; Callot and Guichet, 2003), as *K*1 often results in an intersection axis (the zone axis of sub-fabrics).

In the cases of abnormal magnetic fabrics with *K*1 axes not coincident with the magma flow direction or when *K*1 and *K*3 axes and symmetry are inverted, the relationships between crystal orientation, magma flow direction and principal susceptibilities can be explained (Rochette et al., 1991, 1999) by: (a) single domain effects of magnetite crystals, (b) late growth of ferromagnetic minerals in a direction perpendicular to the dyke-wall, (c) rolling effects on large grains, and (d) turbulent flow.

Homogeneous cooling of tabular magma bodies commonly results in a systematic but variably spaced columnar jointing, related to thermal contraction (Jaeger, 1961; Spry, 1962; Ryan and Sammis, 1978; Kantha, 1981). The magnetic fabric produced by this process is characterized by a random distribution of *K*1 and *K*2 axes on a plane perpendicular to the column axis and the *K*3 axes grouped around the column

* Corresponding author. Fax: +34 976761106.
E-mail address: agil@unizar.es (A. Gil-Imaz).

0191-8141/$ - see front matter © 2006 Elsevier Ltd. All rights reserved.
doi:10.1016/j.jsg.2005.12.016

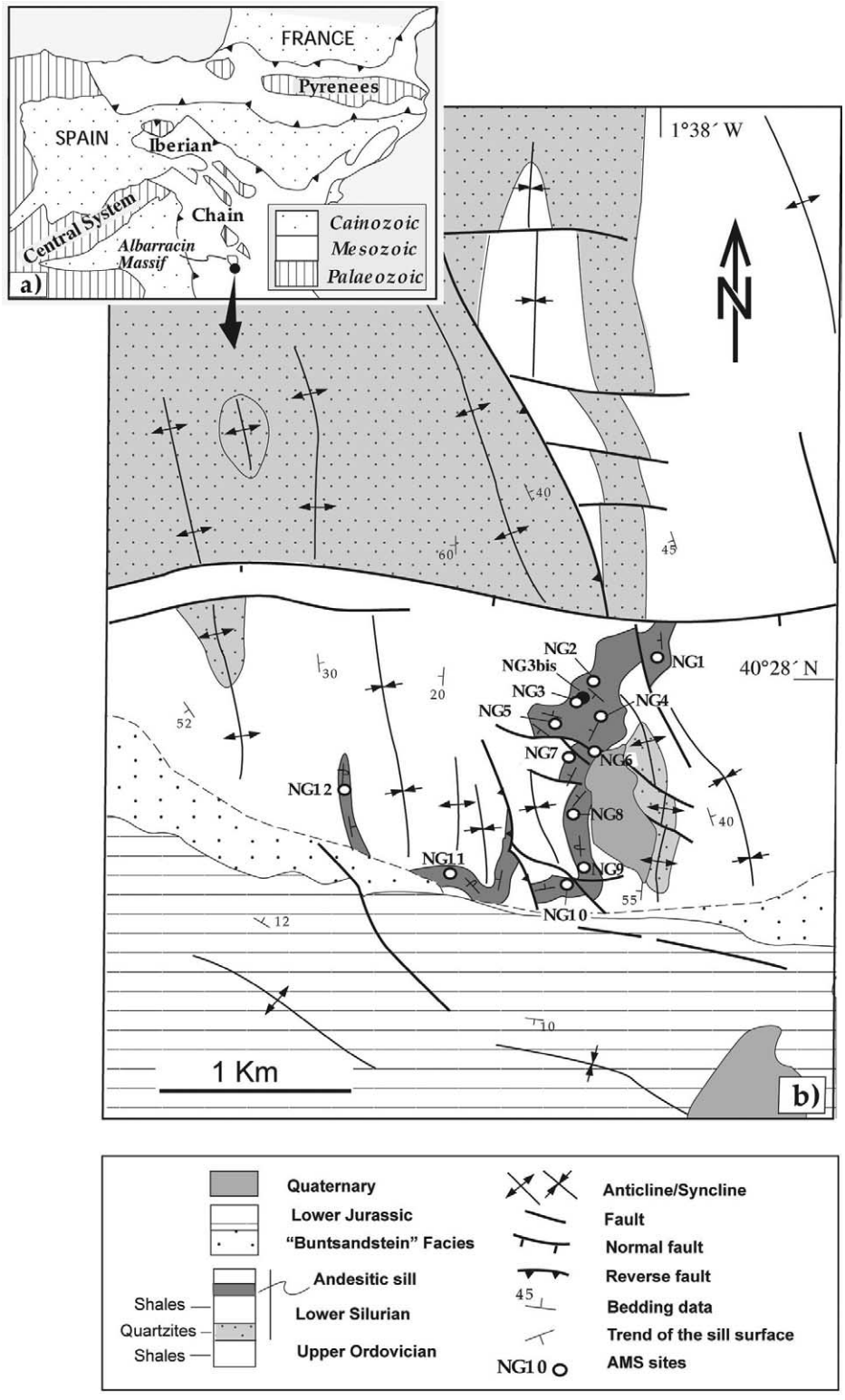

Fig. 1. (a) Location of the Albarracín Massif within the Iberian Chain. (b) Geological map of the studied area and location of the AMS sites.

axis (Brown et al., 1964). Some authors have described a preferred long-axis alignment of magnetic minerals normal to the long axis of the column in response to thermal stresses (Ellwood and Fisk, 1977; Ellwood, 1979). Systematic variations related to column shape are found in bulk susceptibility, anisotropy of shape and anisotropy degree (Urrutia-Fucugauchi, 1982; Urrutia-Fucugauchi et al., 1991). In addition to this, other factors can modify the AMS fabric in tabular igneous bodies during the formation of the columns, as the presence of single domain magnetites, which have an

inverse fabric with respect to the column shape (Potter and Stephenson, 1988), or the grain size variations across the tabular body (MacDonald et al., 1992).

In this paper, the results are presented of a detailed study of the AMS, in a sill of late-Variscan age outcropping in the southeastern part of the Castilian Branch (Iberian Chain, Spain). The sill is folded around a NNW–SSE-trending axis and variably oriented columnar jointing occurs all over the studied area. This outcrop thus represents an interesting case to study the effects of magma flow and thermal processes on the resulting AMS fabric, in a complex geological setting.

2. Regional setting: tectonics, stratigraphy and petrology

The Albarracin Massif is an E–W-trending outcrop of Palaeozoic rocks located in the southeastern part of the Iberian Chain (Northeastern Spain; Fig. 1a). This Massif is mainly composed of a thick sedimentary and low-grade metamorphic series of Ordovician–Silurian age, affected by NNW–SSE-trending Variscan folds (Lozte, 1929; Julivert et al., 1974). Several calc-alkaline extrusive and intrusive igneous bodies (sills, dykes and flows) are emplaced within the Palaeozoic series (Lago et al., 1996, 2004). These igneous rocks are unconformably overlain by Buntsandstein facies (Upper Thüringian–Lower Anisian; López-Gómez and Arche, 1993) red beds. Although the Autunian age of some volcaniclastic outcrops (related to the early Permian extensional stage) has been proved by means of paleontological and absolute age data (Lago et al., 1996, 2004), the structural and stratigraphic features of the studied outcrop suggest an early emplacement of the magma just before the last Variscan folding phase.

From a structural point of view, the studied sill is interbedded within the bottom of a NNW–SSE-trending folded sequence of Silurian age (mainly black shales; Lozte, 1929; Riba, 1959; Portero et al., 1981). The folds are east-verging and gently plunging to the north (Fig. 1b). Both the igneous body and the Variscan folds are cut by a large E–W normal fault to the north and some other minor NW–SE- to E–W-trending normal and reverse faults. To the south, the limit of the Palaeozoic outcrop is the Buntsandstein facies basal unconformity, a regional feature recognized all over the Iberian Chain. The thickness of the sill varies from a maximum of around 70 m to less than 20 m and the exposed area of the sites frequently exceeds 20 m^2. A well-defined jointing, normal to the walls of the sill, affects the sill throughout the outcrop. The joints define polygonal columns with an increasing height/diameter ratio from the contact to the inner part of the sill. The columns are normally limited by four or five sides, although hexagonal sections also occur.

Table 1
Site mean anisotropy susceptibility data for the andesites of Noguera sector

Site	N	K_m	P_j	T_j
NG1	12	265	1.020	0.257
NG2	17	239	1.008	0.265
NG3	16	294	1.015	0.023
NG3bis	82	241	1.012	0.466
NG4	14	291	1.014	−0.313
NG5	14	199	1.010	−0.064
NG6	23	285	1.009	−0.137
NG7.1	12	298	1.010	−0.018
NG7.2	13	262	1.009	−0.050
NG7.3	23	288	1.010	0.273
NG8	11	303	1.012	−0.282
NG9	14	289	1.007	0.147
NG10	14	266	1.009	−0.284
NG11	16	498	1.006	0.181
NG12	14	325	1.012	−0.184

N = number of specimens; K_m = bulk susceptibility ($\times 10^{-6}$ SI units); P_j and T_j are the degree of anisotropy and the symmetry of shape, respectively (Jelinek, 1981).

The petrological study of the sill reveals that the outer margins of the intrusion are composed of fine-grained, porphyritic andesite that progressively grades to coarse dacite in the central parts. The geochemistry of these rocks indicates a calc-alkaline affinity (Lago et al., 1996). The samples analysed in this paper include dacite, dacite–andesite and minor andesite. Primary phases in dacite and dacite–andesite include: zoned plagioclase phenocrysts and microcrysts (35–45%), partially replaced biotite phenocrysts (10–30%), quartz xenocrysts (15–25%) and rare (<1%) or absent amphibole crystals (hornblende). Subidiomorphic magnetite crystals (1–2%), apatite, zircon and tourmaline are common accessory minerals. Secondary phases include chlorite (5–20%), calcite (0–5%) and haematite (0–1%). Andesite samples are characterized by the presence of rare orthopyroxene crystals. Petrographic observations suggest that primary biotite and secondary chlorite are the main paramagnetic phases in all the samples. Euhedral primary magnetite crystals and secondary haematite are the main ferromagnetic phases.

3. Anisotropy of magnetic susceptibility (AMS) study

3.1. Theory of the AMS technique

The AMS technique is based on the measurement of the variation of susceptibility in a standard volume of rock when a weak magnetic field (≤ 1 mT) is applied in different directions. Such a variation can be described mathematically by means of a second-rank symmetric tensor, which can be physically expressed as an ellipsoid whose principal axes represent the three principal susceptibilities (maximum, intermediate and minimum susceptibility axes, or $K1 \geqq K2 \geqq K3$). With independence of the source of the magnetic susceptibility (ferromagnetic, paramagnetic or diamagnetic minerals), it has been demonstrated that the magnitude of this anisotropy depends on two factors: the magnetic anisotropy of the particles themselves and the degree of their alignment (Tarling and Hrouda, 1993). The preferred orientation of crystallographic axes (crystalline anisotropy) determines the AMS for the majority of minerals (mainly in paramagnetic minerals and haematite). In the case of magnetite, the AMS is controlled by the shape preferred orientation of individual grains or grain aggregates (shape anisotropy). The respective contributions of the paramagnetic (silicates) and ferromagnetic (magnetite and other Fe–Ti oxides) phases to the whole AMS depend on both

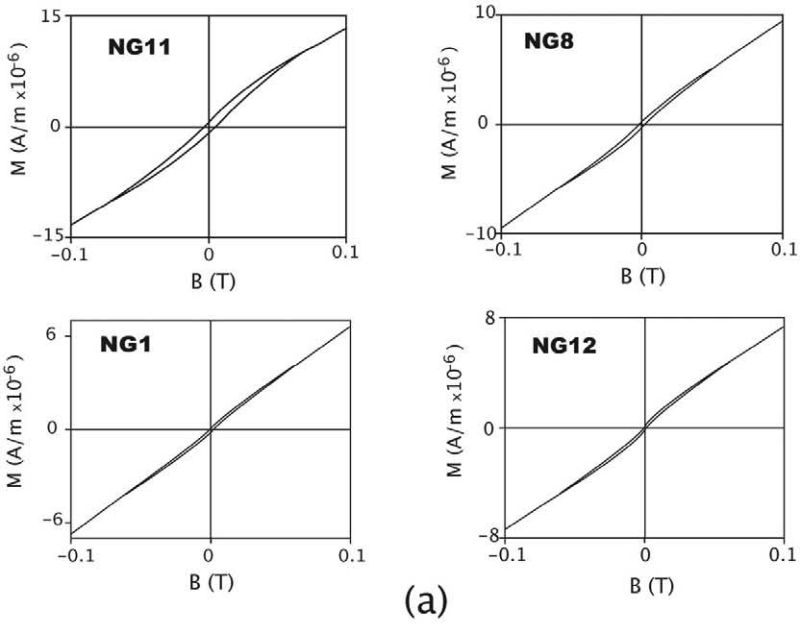
NG11
NG8
NG1
NG12
M (A/m x10⁻⁶)
B (T)
15
0
-15
10
-10
6
-6
8
-8
-0.1
0.1

(a)

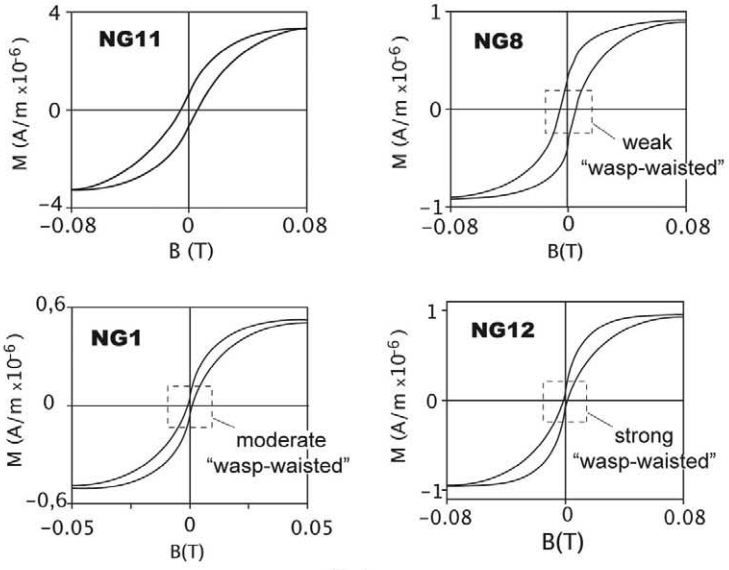
NG11
NG8
NG1
NG12
M (A/m x10⁻⁶)
B (T)
B(T)
weak
"wasp-waisted"
moderate
"wasp-waisted"
strong
"wasp-waisted"
4
-4
1
-1
0,6
-0,6
-0.08
0.08
-0.05
0.05

(b)

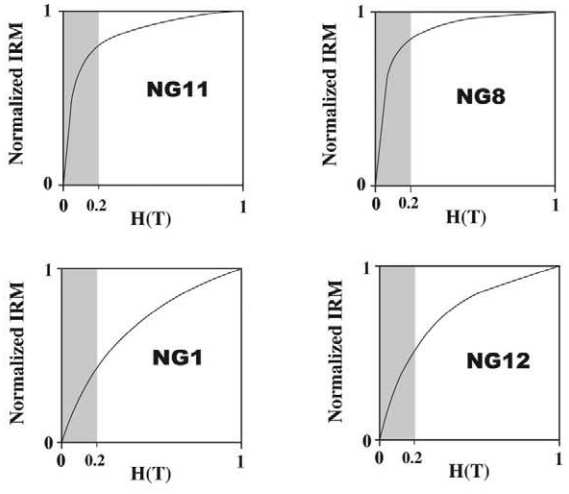
NG11
NG8
NG1
NG12
Normalized IRM
H(T)
1
0
0.2

(c)

the intrinsic susceptibility of the minerals and on their concentration in the rock (Hrouda and Kahan, 1991). For rocks containing a significant modal proportion (ca. 10%) of paramagnetic minerals, Tarling and Hrouda (1993) stated that the AMS of the rock depends mainly on the ferromagnetic minerals if the bulk susceptibility is above 5×10^{-3} [SI], whereas the paramagnetic fraction is the main contributor to the AMS for bulk susceptibilities below 5×10^{-4} [SI].

Many parameters are classically used to describe the AMS fabric of rocks. In this study we use the following parameters to characterize the magnitude and shape of the susceptibility ellipsoid (Jelinek, 1981; Hrouda, 1982):Corrected anisotropy degree:

$$P_j = \exp[2(\eta_1-\eta_m)^2 + (\eta_2-\eta_m)^2 + (\eta_3-\eta_m)^2]^{1/2}$$

where $\eta_1=\ln K_1$, $\eta_2=\ln K_2$, $\eta_3=\ln K_3$ and $\eta_m=(\eta_1+\eta_2+\eta_3)/3$Shape parameter:

$$T_j = [2\ln(K2/K3)/\ln(K1/K3)]-1$$

The P_j parameter is used to quantify the degree of magnetic anisotropy and T_j characterizes the shape of the AMS ellipsoid. In addition to these parameters, we also use the bulk magnetic susceptibility $K_m=(K1+K2+K3)/3$.

Samples for the AMS analysis were collected from 13 sites along the intrusion (Fig. 1b). Three to eight, 6–15 cm long, 2.54 cm diameter oriented cores were drilled at each site using a portable drill. One to four samples with a height/diameter ratio of 0.82 were obtained from each core. AMS was measured with a KLY-2.02 susceptibility meter (using a bridge at low magnetic field), which is based on measuring the directional susceptibilities corresponding to 15 suitable directions in the rock specimens (Jelinek, 1981). The averages (arithmetic mean) of AMS data for all sites are reported in Table 1.

3.2. AMS results

3.2.1. Magnetic susceptibility and magnetic mineralogy

The K_m values of the analysed samples (Table 1) range from 199×10^{-6} [SI] (site NG5) to 498×10^{-6} [SI] (site NG11). The average bulk susceptibility is 235×10^{-6} [SI]. A good correlation exists between the petrology and the bulk susceptibility of the samples, without significant deviations. Dacitic samples have the lowermost values (sites NG5 and NG2) compared with the more andesitic ones (sites NG11 and NG12). Given that both paramagnetic and ferromagnetic phases control the magnetic susceptibility (and its anisotropy) and because the ranges of the bulk susceptibility are not indicative of the precise source of the magnetic properties (i.e. samples with low K_m values could indicate a predominantly ferromagnetic contribution), the determination of the nature and relative contribution of each phase to the bulk susceptibility is necessary in order to understand the origin of the magnetic fabric.

The relative contribution of ferromagnetic and paramagnetic mineral phases to the bulk magnetic susceptibility can be derived from the analysis of the hysteresis curves, following the method by Borradaile and Werner (1994). Hysteresis loops at room temperature were recorded for representative samples using a SQUID magnetometer (model MPMS-5S, Quantum Design). The paramagnetic (K_{para}) contribution to the bulk susceptibility is derived from the slope of the initial hysteresis curves after saturation (between 0.05/0.08 and 0.1 T; Fig. 2a), and is expressed as a percentage of the bulk susceptibility (K_m) on each sample. In the studied samples K_{para} ranges from 20 to 27%. These results support that ferromagnetic phases are the main contributors to the bulk susceptibility in the studied samples, despite their low modal proportions (below 2%), compared with those of the paramagnetic minerals.

The loop for the ferromagnetic component is obtained by substraction of the field independent magnetic susceptibility in the initial hysteresis loop. As shown in the graphs (Fig. 2b), four patterns of corrected hysteresis loops can be inferred. Although the complete saturation at 0.1 T indicates the presence of very low coercivity minerals (i.e. magnetite), the wasp-waisted shape of the curves suggests the combined effect of different ferromagnetic phases (Roberts et al., 1995; Muttoni, 1995).

The isothermal remanent magnetization (IRM) for the same representative specimens was analysed, in order to discriminate the ferromagnetic mineralogy. As shown in the plots (Fig. 2c), the saturation paths (with a steep increase of saturation below 0.2 T and a more gentle increase for higher values) suggest the presence of minerals with both high and low coercive forces. The IRM paths agree with the petrographic observations and the hysteresis results that indicate the presence of both irregular haematite crystals and idiomorphic magnetite crystals. Due to the fairly oxydizing behaviour of the magma, other ferromagnetic phases like maghemite cannot be ruled out as part of the mineral assemblage.

3.2.2. Shape and orientation of the magnetic ellipsoids

The analysis of the shape of the magnetic ellipsoids was performed by means of anisotropy plots where the mean shape (T_j) corresponding to each site is plotted versus the degree of anisotropy (P_j). As shown by the synthetic anisotropy plots (Fig. 3), either oblate or prolate shapes are common in the studied samples. The site mean values of the P_j and T_j parameters vary from 1.02 to 1.006 (1.01 on average) and between $+0.466$ and -0.313, respectively. The very low degree of magnetic anisotropy (P_j below 1.05) agrees with the values found in basaltic–andesitic shallow intrusive rocks (Hrouda, 1982; Staudigel et al., 1992; Tamrat and Ernesto, 1999; Callot et al., 2001) where magnetite is the main carrier of the primary magnetic fabric and the AMS is controlled by

Fig. 2. (a) Initial hysteresis loops, (b) loops with paramagnetic susceptibility substracted and (c) normalized curves of isothermal remanent magnetization (IRM) for four selected samples (sites NG11, NG8, NG1 and NG12).

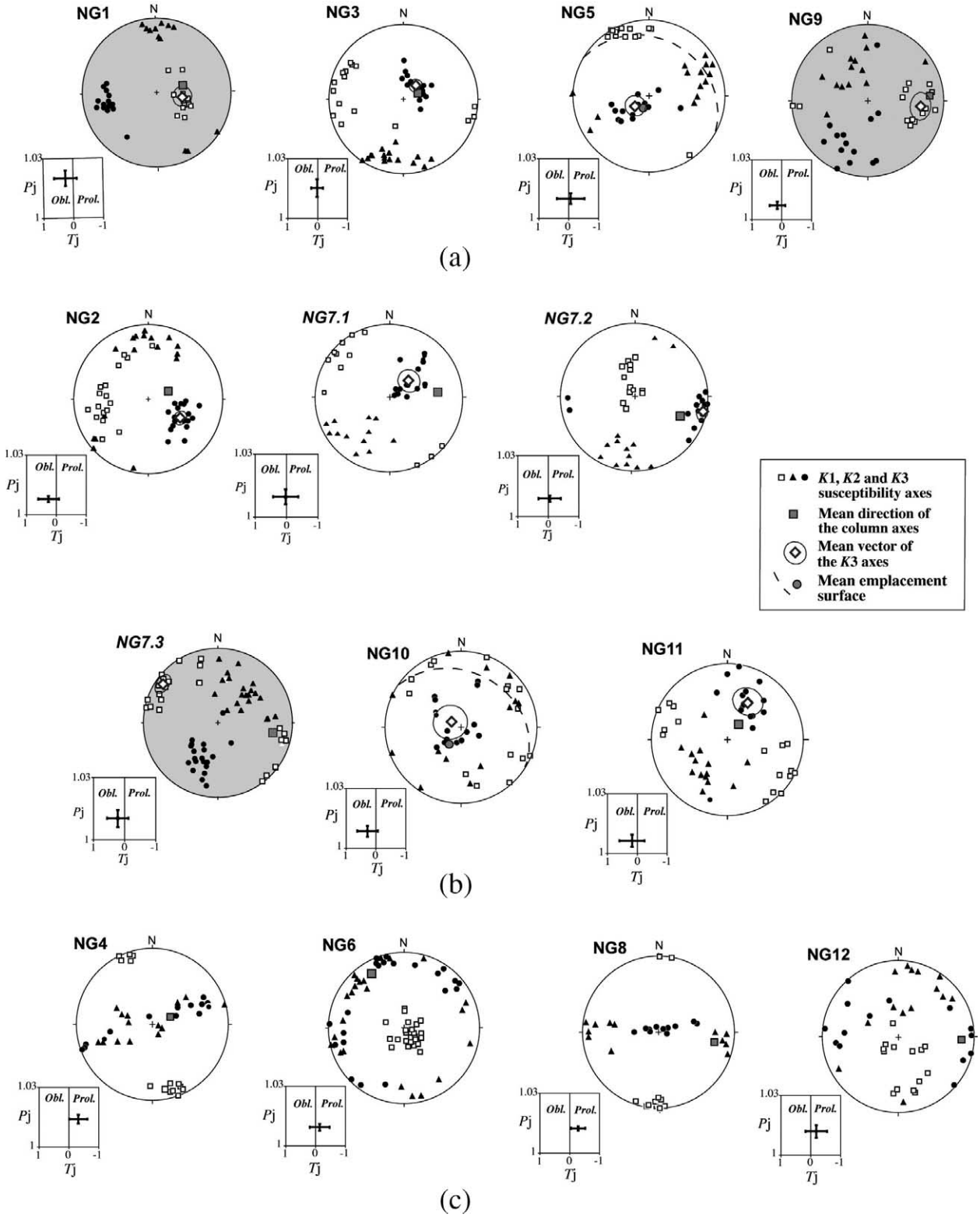

Fig. 3. Stereoplots of AMS directional data and corresponding anisotropy plots for the analysed sites. (a) Sites with oblate ellipsoids and the mean of the $K3$ axes close to both the column axes and the pole of the sill surface. (b) Sites with the magnetic foliation oblique to the sill plane. (c) Sites dominated by prolate ellipsoids. Gray stereoplots correspond to the 'inverse' magnetic fabrics. Error bars in the anisotropy plots represent the standard deviations of the arithmetic mean.

the shape of the grains (shape anisotropy) and their alignment. In the studied samples, textural features such as the presence of sub-isometric magnetite grains are consistent with their very low P_j values.

The values of the shape parameter T_j (Fig. 3) can be either positive or negative, indicating that there is no predominance of magnetic foliation over magnetic lineation, as could be expected for the AMS fabric in tabular intrusions.

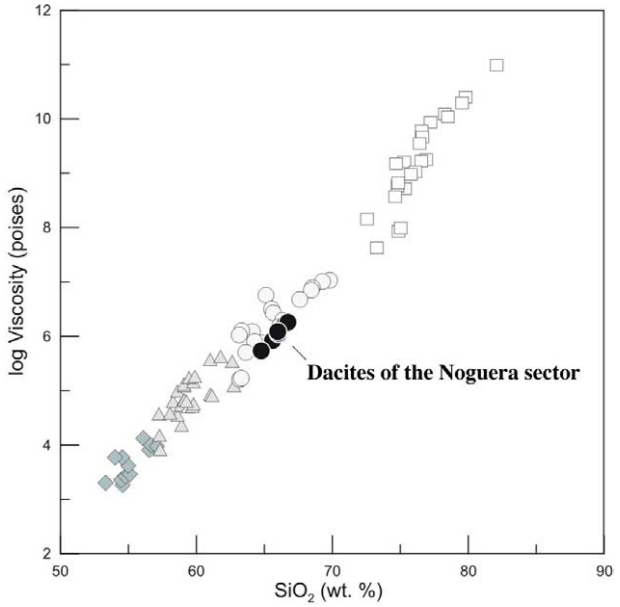

Fig. 4. Calculated viscosity versus SiO_2 content for representative calc-alkaline Permian igneous rocks of the Iberian Chain. Squares: rhyolite; open circles: dacite; triangles: andesite; diamonds: basalt; filled circles: Noguera dacites. Viscosity is the $\log_{10}$ of the liquid viscosity in Poise, calculated assuming a wet magma and a linear evolution of temperature from 1250 °C for 48% SiO_2 and 700 °C for 78% SiO_2 (calculations from McBirney (1993)). Compositions of igneous rocks from the Iberian Chain taken from Lago et al. (1996, 2004).

Nevertheless, some sites are preferentially dominated by oblate ellipsoids, others by prolate ones and some by triaxial ellipsoids ($0.5 \geqq T_j \geqq -0.5$). The variety of ellipsoid shapes, together with directional arguments suggests that the magnetic fabric in different sites along the sill does not reflect a unique and homogeneous process.

The directional analysis of the principal susceptibility axes for each site was performed by means of equal-area stereographic projections (Fig. 3). In order to define the 'normal' or 'inverse' character of the magnetic fabric, we have considered its relationship to the petro-structural elements (i.e. mean direction of the column axes obtained from the direction of the column edges, the emplacement surfaces and the cartographic fold axis). In agreement with Rochette et al. (1991) we define a magnetic fabric as 'normal' when it is characterized by dominant oblate-shaped ellipsoids and a well defined magnetic foliation parallel to the emplacement surface. 'Normal' magnetic fabrics produced by thermal contraction are characterized by a predominance of oblate ellipsoids with the *K3* axes grouped around the column axis (Ellwood and Fisk, 1977; Ellwood, 1979; Urrutia-Fucugauchi et al., 1991). In contrast with this, an 'inverse' magnetic fabric is defined by the grouping of the *K*1 axes parallel to the column axis.

As shown in the stereoplots (Fig. 3), most of the sites have 'normal' magnetic fabrics, with the exception of sites NG1, NG7.3 and NG9, which have 'inverse' fabrics, characterized by a well-defined magnetic lineation around or near to the column axis.

Considering the mean orientation of the magnetic ellipsoids and its average shape, different magnetic patterns can be defined (Fig. 3). Some sites dominated by oblate ellipsoids (Fig. 3a), present a magnetic foliation close to the sill plane. This type includes sites with the mean of the *K*3 axes close to both the column axis (the inverse fabric of sites NG1 and NG9 and the normal fabric of site NG3) and to the pole of the emplacement surface (site NG5). Some other sites with oblate ellipsoids show the magnetic foliation oblique to the sill plane (i.e. the mean of the *K*3 axes oblique to both the column axis and the pole of the emplacement surface). This second group includes the normal fabric of sites NG2, NG7.1, NG7.2, NG10, NG11 and the inverse fabric of site NG7.3 (Fig. 3b). Finally, four sites are characterized by prolate ellipsoids (sites NG4, NG6, NG8 and NG12) and without magnetic foliation (Fig. 3c).

4. Origin of the magnetic patterns

As previously stated, both the bulk susceptibility and the magnetic anisotropy of the studied samples are produced by different ferromagnetic minerals (K_{ferro} ranges from 73 to 80%). Textural features of the rock-fabric (sub-idiomorphic magnetite crystals included within primary silicates like plagioclase and biotite phenocrysts) suggest that the magnetite crystals in the rock matrix crystallized during the early cooling history of the rock. Although the wasp-waisted shape of the corrected hysteresis loops indicates a mixture of high- and very low-coercivity minerals, the magnetic analysis suggests the predominance of weakly anisotropic minerals like magnetite. From the analysis of directional data and taking into account the relationship between the magnetic fabric and the petro-structural indicators, it works out that the magnetic fabric of these samples is due to early-crystallized magnetite grains and, on the other hand, the reorganization of the primary magnetic fabric can be related to other post-emplacement processes.

4.1. Magma flow

The effect of a static wall during the movement of the magma within an opening discontinuity is usually recognized in the imbricated scheme of the AMS foliations (Knight and Walker, 1988; Hillhouse and Wells, 1991; Cañón-Tapia et al., 1996; Walker et al., 1999; Geoffroy et al., 2002). According to this, the magnetic patterns of sites NG2, NG7.1, NG7.2, NG7.3, NG10 and NG11 (Fig. 3b), with a magnetic foliation oblique to the petrostructural elements (i.e. both the sill wall and the column axes), can be interpreted as the result of a magma flow effect. The angle of obliquity between the magnetic foliation and the sill wall was measured taking as a reference the mean direction of the *K3* axes and either the pole of the average emplacement surface directly measured on site or the orientation of the column axes (accepting that they are perpendicular to the sill wall). Both for the emplacement surfaces and the column axes, the orientation data measured in the field were averaged to reduce local errors.

The acquisition of magmatic fabrics is controlled by two critical factors: the viscosity of the magma, which controls the flow velocity and regime (laminar or turbulent), and the timing

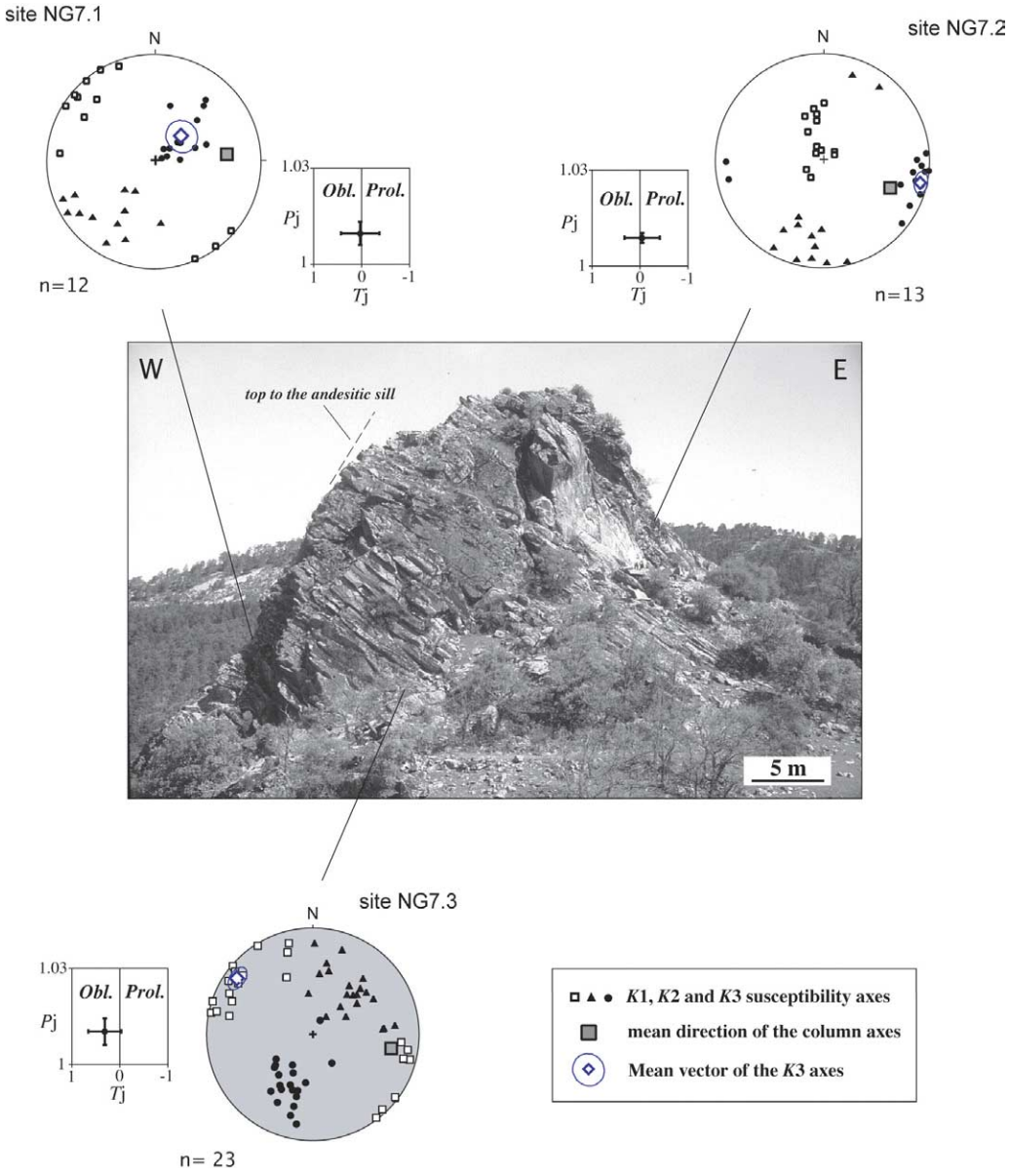

Fig. 5. Panoramic view of the Noguera andesitic sill. Note its high tilt to the west. Stereograms of directional data and anisotropy plots for three sites located at different distances from the top of the sill are reported. Gray stereoplot indicate the 'inverse' magnetic fabric of site NG7.3. Error bars in the anisotropy plots represent the standard deviations of the arithmetic mean.

of crystallization of the ferromagnetic minerals in the rock. Crystallizing magmas with less than 30% of crystals (viscosities below 10^4 poise; Fernández and Gasquet, 1994) behave as Newtonian liquids and do not develop mineral preferred orientations. Above this rheological threshold, the behaviour of magma corresponds to that of a Binghamian liquid and the magnetic fabric develops as a result of rigid-body rotations of crystals (Fernández and Gasquet, 1994; Hrouda et al., 1999). The timing of crystallization of the ferromagnetic phases influences their behaviour, which can be passive for early crystals or active, with crystallization coeval to flow. In the studied sill, with a moderate estimated magma viscosity in the range 5×10^5–3×10^6 poise (Fig. 4), the magnetic fabric can be interpreted as the result of the passive rotation of early-crystallized sub-equant magnetites.

Additional evidence of such an imbricate model of magma flow is seen in sites NG7.1, NG7.2 (with a normal magnetic fabric) and NG7.3 (with an inverse fabric). As shown in Fig. 5, the magnetic foliation is oblique to the sill wall (i.e. the mean of the *K*3 axes is oblique to the mean of the column axes) and a gradual decreasing in the obliquity angle from site NG7.1 (located near the sill wall) to site NG7.2 (located in the inner part of the sill) ocurrs. This variation of the magnetic pattern from the outer to the inner parts of the igneous mass is consistent with a decrease of the wall effect (and of the shear responsible for the imbrication) towards the inner part of the sill. This pattern of internal fabric is consistent with a 'cooling-related Binghamian' dyke model (non-Newtonian magma), in which the magmatic foliation becomes parallel to the flow vector in the core of the dyke (Komar, 1972a,b, 1976).

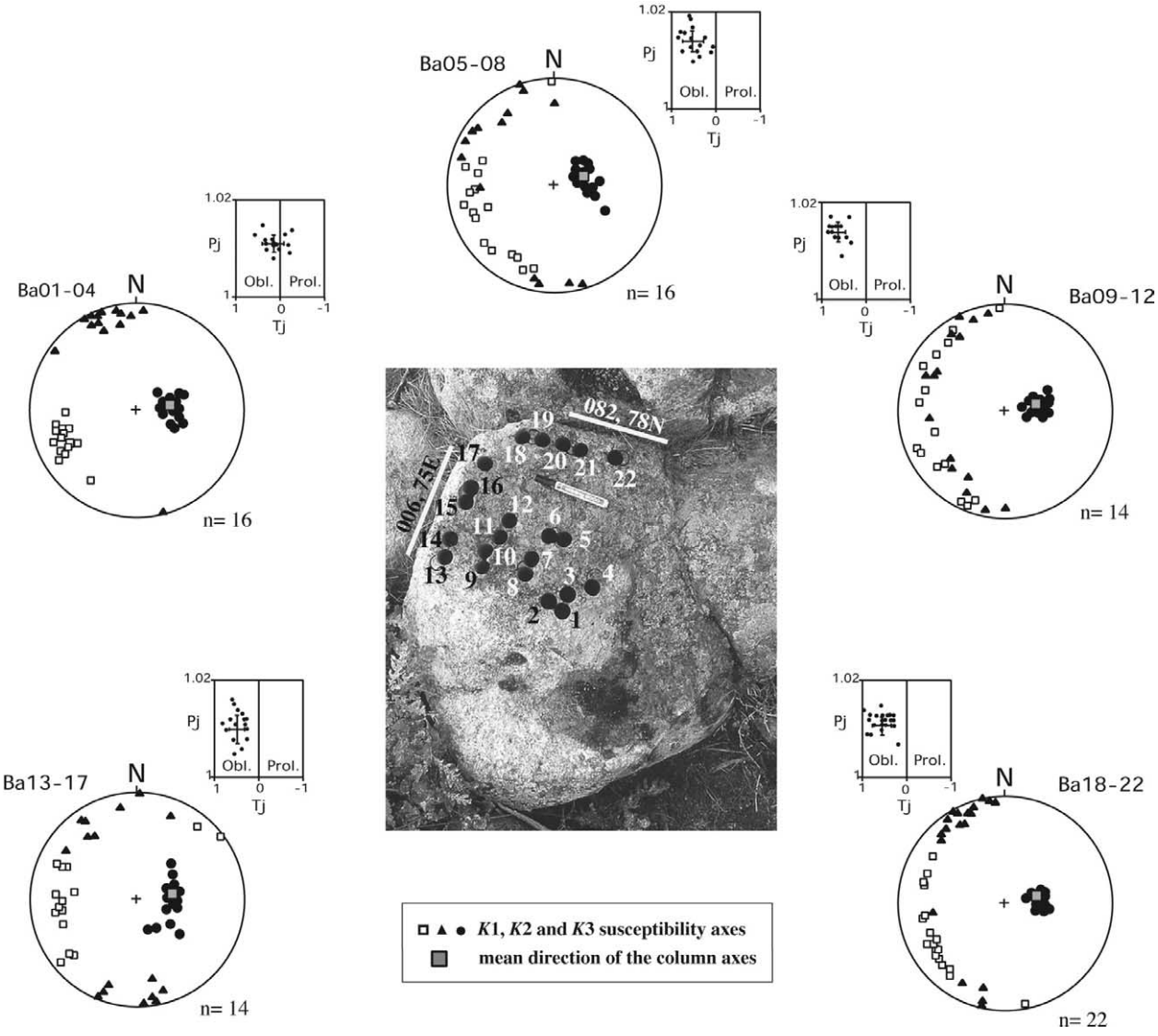

Fig. 6. Bottom of a sampled andesitic column: Site NG3bis. The stereographic projections of the susceptibility axes and the anisotropy plots for all the samples are shown.

In addition to the obliquity between the magnetic foliation and the sill wall, the presence of prolate magnetic fabrics in sheet-like intrusions is a feature commonly interpreted as related to magma flow kinetics; in most of these cases, the magnetic lineation is parallel to the flow direction (Ellwood and Fisk, 1977; Ellwood, 1978; Knight and Walker, 1988; Ferré et al., 2002). Thus the magnetic pattern from sites NG4, NG6, NG8 and NG12 (Fig. 3c), in which a magnetic lineation is defined on the plane parallel to the sill surface (normal to the column axis), suggests its primary origin linked to magma flow.

4.2. Thermal contraction

In order to determine the contribution of thermal contraction processes to the magnetic fabric, a centre to border sampling of a single column from site NG3 (site named NG3bis) was carried out (Fig. 6). A total of 22 cores (82 specimens) coming from the top of a single column were collected (Table 2). As shown by the anisotropy plots and directional data of the susceptibility axes, the ellipsoid shapes (and magnetic anisotropy) and the directional patterns vary gradually from

Table 2
Site mean anisotropy susceptibility data for samples from the bottom of an andesitic column of site NG3bis

Sample	N	K_m	P_j	T_j
Ba01–Ba04	16	234	1.011	0.14
Ba05–Ba08	16	235	1.014	0.51
Ba09–Ba12	14	279	1.014	0.63
Ba13–Ba17	14	240	1.010	0.48
Ba18–Ba22	22	219	1.011	0.57

N = number of specimens; K_m = bulk susceptibility ($\times 10^{-6}$ SI units); P_j and T_j are the degree of anisotropy and the symmetry of shape, respectively (Jelinek, 1981).

the centre to the border. Samples from the centre of the column have well defined triaxial magnetic ellipsoids and a magnetic lineation, whereas the samples from the border are characterized by more oblate ellipsoids.

The early crystallization of magnetite (the main carrier of the magnetic anisotropy) in the studied rocks makes this mineral suitable for recording any other processes affecting the magma and, later, the resulting rock. The magnetic lineation observed in the central cores can be interpreted as a primary feature, related to magma flow. After the emplacement, thermal contraction could explain the coaxial gradual change of the magnetic fabric from the centre to the border of the column, as the thermal stresses linked to contraction gradually decrease from the border to the centre, where the original magmatic lineation is preserved. The magnetic fabric linked to thermal contraction must be related to near-solidus passive rotation of early magnetite crystals, within the relatively viscous igneous mass.

These single-column results are consistent with the rest of the data measured for site NG3 (Fig. 3a), (See the high degree of coaxiality between the mean direction of K 3 axis and the column axes). This magnetic pattern also occurs in other sites where the columns are better developed (sites NG1, NG5 and NG9 in Fig. 3a) suggesting that the original flow-related fabric is variably overprinted by the thermal contraction process in these sites.

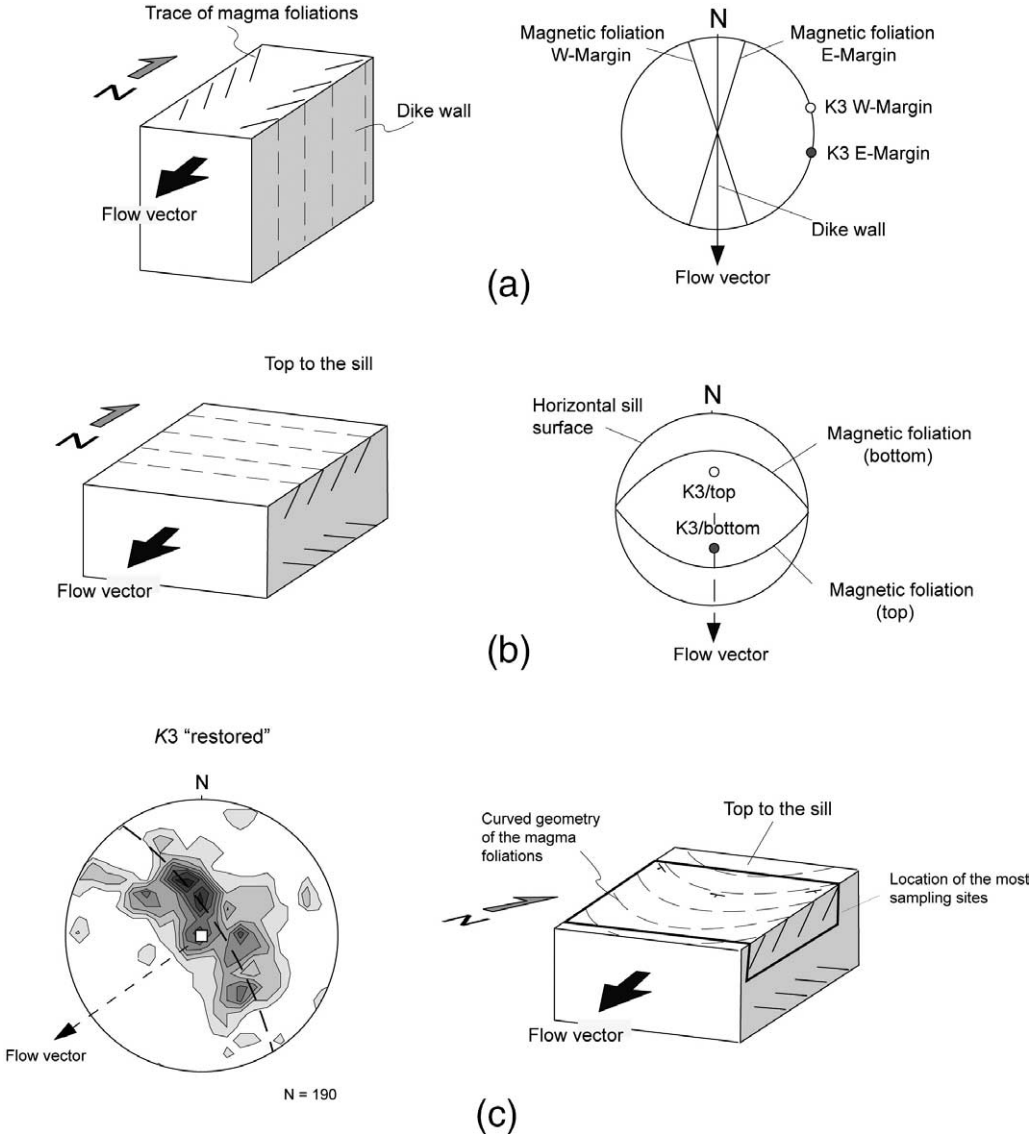

Fig. 7. Flow vector determination. Theoretical sketch and corresponding stereoplot of flow vector determination for a dyke (a) and sill (b). (c) Interpretation of the flow vector in the studied sill from the directional pattern of the restored $K3$ axes. For data coming from the top of the sill, the flow vector coincides with the normal to the girdle of the $K3$ axes. Concerning the frequency stereoplot, data coming from the swapping of $K1$ and $K3$ axes corresponding to the 'inverse' magnetic fabrics have been also considered. Due to the structural complexity linked to post-folding fracturing data from site NG6 have not been included (see the cartographic fault affecting this site in Fig. 1). Contour intervals are 0.7%. Equal area, lower hemisphere.

5. Interpretation of the AMS fabric: discussion

According to Henry (1997), a remarkable feature of the AMS in tabular intrusions, which is also present in some of the studied sites, is that the magnetic lineation represents the zone axis of the magnetic foliations. This implies that *K*1 axes are not unequivocal flow direction markers and only the *K*3 axes can be used for such purposes (Hillhouse and Wells, 1991; Geoffroy et al., 2002). In order to evaluate the effect of the primary magma flow in the studied samples at a regional scale we have plotted the whole susceptibility directional data, corresponding only to the *K*3 susceptibility axes in its 'restored' position. Restored data were obtained applying the plunge correction to both the cartographic fold axis and to each individual column.

The flow vector in dykes can be calculated using only their magnetic foliations (Geoffroy et al., 2002). These authors stated that, in vertical dykes, the flow vector could be defined completely by the perpendicular to the axis intersection between the magnetic foliation and the dyke wall (Fig. 7a). In sills with horizontal parallel walls, or when restoring the structure of dipping sills to the horizontal, the flow vector would be contained in a vertical plane perpendicular to the strike of the magnetic foliations measured on each sill wall (Fig. 7b). In both cases, the relationship between the magnetic foliation and the flow vector is clearly defined. The expected scheme for horizontal sills does not occur in the studied case. As shown in the frequency stereogram of restored *K*3 axes (Fig. 7c), the poles of the magnetic foliations (*K*3 axes) are dispersed along a NW–SE girdle inclined to the east. As these directional data correspond to the restored position of the *K*3 axes (the square in Fig. 8c indicates the original vertical position of the columns), the dispersion could be interpreted as an original feature of the AMS fabric. Taking into account that most of the sites were drilled out from the top of the sill, the girdle of *K*3 axes is consistent with a curved geometry of the original magma foliation at a regional scale (and consistent with the velocity distribution model) and then the related flow vector can be inferred from the normal to the girdle (Fig. 7c). The observed low-symmetry pattern of the distribution of the *K*3 axes is related to the sampling representativity, limited by the outcropping surfaces.

Instead of a well-defined magnetic lineation linked to magma flow, dispersion of the *K*1 axes on the magnetic foliation is evident in some sites (see site NG3bis on Fig. 6 and sites NG2, NG7.2, NG11 and NG12 on Fig. 3). This pattern cannot be explained as the consequence of a turbulent flow of the magma, as this kind of process typically produces random orientations of all the susceptibility axes (Knight and Walker, 1988). Moreover, the radial pattern of the stresses linked to thermal contraction could explain the dispersion of *K*1 axes within the flow plane, during the late stages of magma crystallization. In contrast with the regional-scale magma flow process, the effects of thermal contraction are probably significant only at the site/column scale.

The ENE–WSW folding responsible for NNW–SSE-trending cartographic folds in the studied area is the last identifiable process that affected the sill. Its passive effect on the magnetic fabric is supported by the directional pattern of the 'in situ' *K*3 susceptibility axes, obtained from the whole dataset (Fig. 8). As shown in the synthetic stereoplot, a main ENE–WSW girdle (whose pole is close to the mean cartographic fold axis) of the *K*3 axes is defined (Fig. 8a). This is consistent with a passive folding of previous surfaces with a predominant ENE–WSW orientation (Fig. 7c), as a result of the process responsible for the cartographic folds (Fig. 8b).

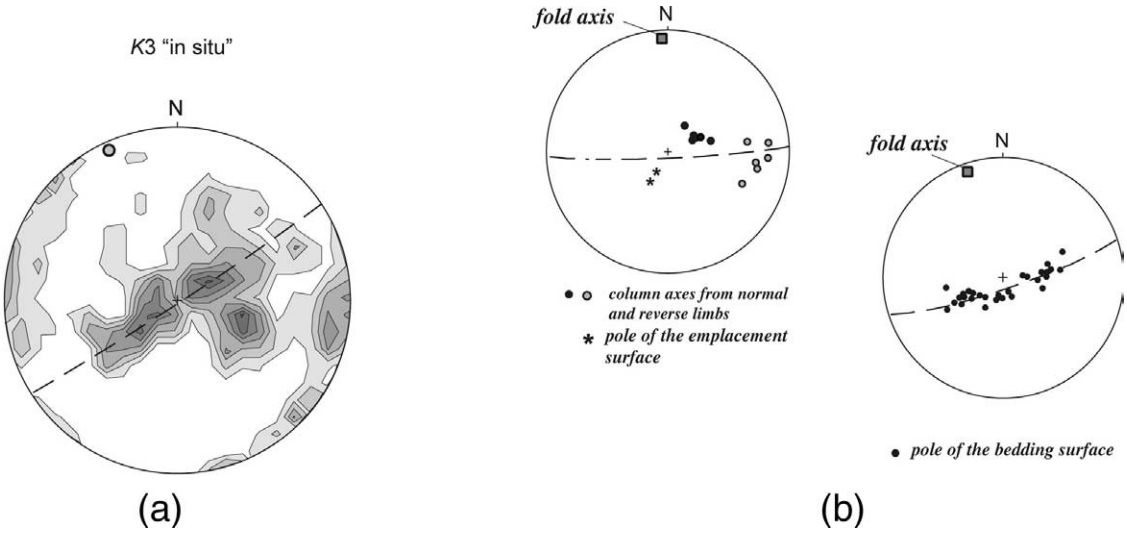

Fig. 8. (a) Frequency stereogram of 'in situ' data of the *K*3 susceptibility axes corresponding to the whole of the analysed specimens (data corresponding to site NG3bis not included). Data coming from the swapping of *K*1 and *K*3 axes corresponding to the 'inverse' magnetic fabrics have been also considered. Due to the structural complexity linked to post-folding fracturing data from site NG6 have not been included (see the cartographic fault affecting this site in Fig. 1). (b) Stereographic projections corresponding to both the cartographic fold affecting the sill (left) and to the Ordovician succession (right). Contour intervals are 0.7%. Equal area, lower hemisphere.

6. Conclusions

This study is focussed on samples collected from 13 sites scattered over the outcropping surface of a folded andesitic sill. This intrusion is one of a large number of late-Variscan calc-alkaline intrusive and extrusive igneous rocks that were emplaced within the Palaeozoic sequences of the southeastern part of the Iberian Chain (Spain). The analysis of magnetic fabrics (AMS) of these rocks reveals a sequence of petrostructural events including: (1) magma flow, (2) near-solidus thermal contraction of the igneous mass, and (3) later folding. Geochemical data and textural evidences indicate that the AMS fabric of these rocks is related to early crystallization of magnetite grains within a medium-viscosity calc-alkaline magma.

From the pattern of the 'restored' $K3$ susceptibility axes obtained for the whole dataset, a horizontal SW-trending flow vector can be deduced. This magnetic pattern is defined by a NW–SE girdle, which reflects an original curved geometry of the magmatic foliation. The observed gradual decrease of the obliquity between the sill plane and the mean magnetic foliations from the contacts of the sill to its interior supports an imbricate scheme of the magnetic fabric.

Thermal contraction linked to lava cooling explains the clustering of $K3$ susceptibility near the mean direction of the column axis. Its effect is more remarkable in sites where well developed polygonal columns occur. A detailed study of a single column has shown that the gradual variation of the magnetic parameters from the border to the centre of the columns is related with thermal contraction. The thermal stresses related to the formation of the columns will explain the absence of a main magnetic lineation within the magnetic foliation. A passive rotation of the early crystallized magnetite grains allows an explanation of the active role of the thermal contraction in the acquisition of the magnetic fabric.

Late folding of the sill produced the rigid-body rotation of the magnetic mineralogy. This statement is supported by the directional pattern of the 'in situ' $K3$ susceptibility axes that records the main structural directions of the cartographic folds.

Acknowledgements

Measurements of AMS and IRM data were carried out at the Institute of Earth Sciences 'Jaume Almera', C.S.I.C. (Barcelona, Spain), using a susceptibility bridge Kappabridge KLY-2.02 and a Pulse magnetizer. Hysteresis measurements were carried out at the Institute of Materials Science of Aragon (ICMA), CSIC-University of Zaragoza, Spain. We gratefully acknowledge the suggestions and constructive criticism of Prof. L. Geoffroy and those of the anonymous reviewer, which helped to improve the manuscript. This work is included in the objectives, and supported by the research project BTE2002-04168-C03-01 (DGES, Spanish Ministry of Education). Financial support from the University of Zaragoza and from CSIC (PAI2003) is acknowledged.

References

Borradaile, G., Werner, T., 1994. Magnetic anisotropy of some phyllosilicates. Tectonophysics 235, 223–248.

Brown, H.C., Khan, M.A., Stacey, F.D., 1964. A search for flow structure in columnar basalt using magnetic anisotropy measurements. Pure and Applied Geophysics 57, 65–71.

Callot, J.P., Geoffroy, L., Aubourg, C., Pozzi, J.P., Mege, D., 2001. Magma flow directions of shallow dykes from the East Greenland volcanic margin inferred from magnetic fabric studies. Tectonophysics 335, 313–329.

Callot, J.P., Guichet, X., 2003. Rock texture and magnetic lineation in dykes: a simple analytical model. Tectonophysics 366, 207–222.

Cañón-Tapia, E., Walker, G.P.L., Herrero-Bervera, E., 1996. The internal structure of lavas: insights from AMS measurements I: near vent 'a–a'. Journal of Volcanology and Geothermal Research 70, 21–36.

Ellwood, B.B., 1978. Flow and emplacement direction determined for selected basaltic bodies using magnetic susceptibility anisotropy measurements. Earth and Planetary Science Letters 41, 254–264.

Ellwood, B.B., 1979. Anisotropy of magnetic susceptibility variations in Icelandic columnar basalts. Earth and Planetary Science Letters 42, 209–212.

Ellwood, B.B., Fisk, M.R., 1977. Anisotropy of magnetic susceptibility variations in a single Icelandic columnar basalt. Earth and Planetary Science Letters 35, 116–122.

Ernst, R.E., Baragar, W.R.A., 1992. Evidence from magnetic fabric for the flow pattern of magma in the MacKenzie giant radiating dyke swarm. Nature 356, 511–513.

Fernández, A.N., Gasquet, D.R., 1994. Relative rheological evolution of chemical contrasted coeval magmas: example of the Tichka plutonic complex (Morocco). Contribution in Mineralogy and Petrology 116, 316–326.

Ferré, E.C., Bordarier, C., Marsh, J.S., 2002. Magma flow inferred from AMS fabrics in a layered mafic sill, Insizwa, South Africa. Tectonophysics 354, 1–23.

Geoffroy, L., Callot, J.P., Aubourg, C., Moreira, M., 2002. Magnetic and plagioclases linear fabric discrepancy in dykes: a new way to define the flow vector using magnetic foliation. Terra Nova 14, 183–190.

Glen, J.M., Renne, P.R., Milner, S.C., Coe, R.S., 1997. Magma flow inferred from anisotropy of magnetic susceptibility in the coastal Paraná–Etendeká igneous province: evidence for rifting before flood volcanism. Geology 25, 1131–1134.

Henry, B., 1997. The magnetic zone axis: a new element of magnetic fabric for the interpretation of the magnetic lineation. Tectonophysics 271, 325–351.

Herrero-Bervera, E., Cañón-Tapia, E., Walker, G.P.L., Tanaka, H., 2001. Magnetic fabric study and inferred flow directions of lavas of the Old Pali Road, Oáhu, Hawaii. Journal of Volcanology and Geothermal Research 118, 161–171.

Hillhouse, J.W., Wells, R.E., 1991. Magnetic fabric, flow direction and source area of the lower Miocene Peach Spring Tuff in Arizona, California and Nevada. Journal of Geophysical Research 96, 12443–12460.

Hrouda, F., 1982. Magnetic anisotropy and its application in geology and geophysics. Geophysical Survey 5, 37–82.

Hrouda, F., Kahan, S., 1991. The magnetic fabric relationship between sedimentary and basement nappes in the High Tatra Mountains, N. Slovakia. Journal of Structural Geology 13, 431–442.

Hrouda, F., Táborska, S., Schulmann, K., Jezek, J., Dolejs, D., 1999. Magnetic fabric and rheology of co-mingled magmas in the Nasavrky Plutonic Complex (E. Bohemia): implications for intrusive strain regime and emplacement mechanism. Tectonophysics 307, 93–111.

Jaeger, J.C., 1961. The cooling of irregularly shaped igneous bodies. American Journal of Sciences 259, 721–734.

Jelinek, V., 1981. Characterization of the magnetic fabric of rocks. Tectonophysics 79, 63–67.

Julivert, M., Fontbote, J.M., Ribero, A., Coned, C., 1974. Mapa tectónico de la Península Ibérica y Baleares. IGME, pp. 1–13.

Kantha, L.H., 1981. "Basalt fingers": origin of columnar joints? Geological Magacine 118 (3), 251–264.

Knight, M.D., Walker, G.P.L., 1988. Magma flow directions in flows of the Koolau Complex, Oahu, determined from magnetic fabric studies. Journal of Geophysical Research 93, 4308–4319.

Komar, P.D., 1972a. Mechanical interactions of phenocrysts and flow differentiation of igneous dykes and sills. Geological Society of America Bulletin 83, 973–988.

Komar, P.D., 1972b. Flow differentiation in igneous dykes and sills; profiles of velocity and phenocryst concentration. Geological Society of America Bulletin 83 (11), 3443–3447.

Komar, P.D., 1976. Phenocryst interactions and the velocity profile of magma flowing through dykes or sills. Geological Society of America Bulletin 83 (9), 1336–1342.

Lago, M., Gil-Imaz, A., Pocoví, A., Arranz, E., Bastida, J., Auqué, L., Lapuente, M.P., 1996. Rasgos geológicos del magmatismo autuniense en la Sierra de Albarracín (Cadena Ibérica occidental). Cuadernos de Geología Ibérica 20, 139–157.

Lago, M., Arranz, E., Pocoví, A., Galé, C., Gil-Imaz, A., 2004. Lower magmatism of the Iberian Chain, Central Spain, and its relationship to extensional tectonics. In: Wilson, M., Neumann, E.R., Davies, G.R., Timmerman, M.J., Heeremans, M., Larsen, B.T. (Eds.), Permo-Carboniferous Magmatism and Rifting in Europe Society, London, Special Publications 223, pp. 465–490.

López-Gómez, J.J., Arche, A., 1993. Sequence stratigraphic analysis and palaeogeographic interpretation of the Buntsandstein and Muschelkalk facies (Permo-Triassic) in the SE Iberian Range, E Spain. Palaeogeography, Palaeoclimatology, Palaeoecology 103, 179–201.

Lozte, F., 1929. Stratigraphie und Tektonik des Keltibersichen Grund-gebirges (Spanien). Beitr. Westl. Mediterrangebiete, 3. Abh. Ges. Wiss. Gottingen. Math. Phys. K.I.N.F., 24(2). Berlin. In: Publicaciones Extranjeras de Geología de España. Institución 'Lucas Mallada' 8, 315pp.

MacDonald, W.D., Palmer, H.C., Hayatsu, A., 1992. Egan Range Volcanic Complex, Nevada: geochronology, paleomagnetism and magnetic fabrics. Physics of the Earth and Planetary Interiors 74, 109–126.

McBirney, A.R., 1993. Igneous Petrology, 2nd ed. Jones & Bartlett Publishers, Boston. 508pp.

Muttoni, G., 1995. "Wasp-waisted" hysteresis loops from pyrrhotite and magnetite-bearing remagnezited Triassic limestone. Geophysical Research Letters 22 (3), 3167–3170.

Portero, J.M., Gutiérrez, M., Aguilar, M.J., Ramírez, J., Aragonés, Giner, J., Riba, O., 1981. Memoria explicativa de la Hoja número 565 (Tragacete) del mapa geológico de España E: 1:50.000, Madrid.

Potter, D.K., Stephenson, A., 1988. Single-domain particles in rocks and magnetic fabric analysis. Geophysical Research Letters 15, 1097–1100.

Riba, O. 1959. Estudio geológico de la Sierra de Albarracín. C.S.I.C. Monografía de la Institución "Lucas Mallada" 16, 238 p.

Roberts, A., Cui, Y., Verosub, K.L., 1995. Wasp-waisted hysteresis loops: mineral magnetics characteristics and discrimination of components in mixed magnetic systems. Journal of Geophysical Research 100, 17909–17924.

Rochette, P., Jenatton, L., Dupuy, C., Boudier, F., Reuber, I., 1991. Emplacement modes of basaltic dykes in the Oman ophiolite: evidence from magnetic anisotropy with reference to geochemical studies. In: Peters, T.J. (Ed.), Ophiolite Genesis and the Evolution of the Oceanic Lithosphere. Kluwer, Dordrecht, pp. 55–82.

Rochette, P., Aubourg, C., Perrin, M., 1999. Is this magnetic fabric normal? A review and case studies in volcanic formations. Tectonophysics 307, 219–234.

Ryan, R.A., Sammis, C.G., 1978. Cyclic fracture mechanisms in cooling basalt. Geological Society of American Bulletin 89, 1295–1308.

Spry, A., 1962. The origin of columnar joints, particularly in basalts flows. Journal of the Geological Society. Austria 8, 191–216.

Staudigel, H.G., Gee, G., Tauxe, L., Varga, R.J., 1992. Shallow intrusive direction of sheeted dykes in the Troodos ophiolite: anisotropy of magnetic susceptibility and structural data. Geology 20, 841–844.

Tamrat, E., Ernesto, M., 1999. Magnetic fabric and rock-magnetic carácter of the Mesozoic flood basalts of the Paraná Basin, Brazil. Journal of Geodynamics 28, 419–437.

Tarling, D.H., Hrouda, F., 1993. The Magnetic Anisotropy of Rocks. Chapman & Hall, London. 217pp.

Urrutia-Fucugauchi, J., 1982. Magnetic anisotropy study of a columnar basalt from San Anton, Morelos, Mexico. Bulletin of Volcanology 45 (1), 1–8.

Urrutia-Fucugauchi, J., Böhnel, H., Negendak, J.F.W., 1991. Magnetic properties and domain state of titanomagnetites in a columnar basalt from Mexico. Journal of Geomagnetism and Geoelectricity 43, 189–205.

Varga, R.J., Gee, J.S., Staudigel, H., Tauxe, L., 1998. Dykes surfaces lineations as magma flow indicators within the sheeted dyke complex of the Troodos ophiolite, Cyprus. Journal of Geophysical Research 103, 5241–5256.

Walker, G.P.L., Cañom-Tapia, E., Herrero-Bervera, E., 1999. Origin of vesicle layering and double imbrication by endogenous growth in the Birkett basalt flow (Columbia river plateau). Journal of Volcanology and Geothermal Research 88, 15–28.